NASA/TM—2015-218924

A First Look at the DGEN380 Engine Acoustic Data From a Core-Noise Perspective

Lennart S. Hultgren
Glenn Research Center, Cleveland, Ohio

December 2015

NASA STI Program . . . in Profile

Since its founding, NASA has been dedicated to the advancement of aeronautics and space science. The NASA Scientific and Technical Information (STI) Program plays a key part in helping NASA maintain this important role.

The NASA STI Program operates under the auspices of the Agency Chief Information Officer. It collects, organizes, provides for archiving, and disseminates NASA's STI. The NASA STI Program provides access to the NASA Technical Report Server—Registered (NTRS Reg) and NASA Technical Report Server—Public (NTRS) thus providing one of the largest collections of aeronautical and space science STI in the world. Results are published in both non-NASA channels and by NASA in the NASA STI Report Series, which includes the following report types:

- TECHNICAL PUBLICATION. Reports of completed research or a major significant phase of research that present the results of NASA programs and include extensive data or theoretical analysis. Includes compilations of significant scientific and technical data and information deemed to be of continuing reference value. NASA counter-part of peer-reviewed formal professional papers, but has less stringent limitations on manuscript length and extent of graphic presentations.

- TECHNICAL MEMORANDUM. Scientific and technical findings that are preliminary or of specialized interest, e.g., "quick-release" reports, working papers, and bibliographies that contain minimal annotation. Does not contain extensive analysis.

- CONTRACTOR REPORT. Scientific and technical findings by NASA-sponsored contractors and grantees.

- CONFERENCE PUBLICATION. Collected papers from scientific and technical conferences, symposia, seminars, or other meetings sponsored or co-sponsored by NASA.

- SPECIAL PUBLICATION. Scientific, technical, or historical information from NASA programs, projects, and missions, often concerned with subjects having substantial public interest.

- TECHNICAL TRANSLATION. English-language translations of foreign scientific and technical material pertinent to NASA's mission.

For more information about the NASA STI program, see the following:

- Access the NASA STI program home page at http://www.sti.nasa.gov

- E-mail your question to help@sti.nasa.gov

- Fax your question to the NASA STI Information Desk at 757-864-6500

- Telephone the NASA STI Information Desk at 757-864-9658

- Write to:
  NASA STI Program
  Mail Stop 148
  NASA Langley Research Center
  Hampton, VA 23681-2199

NASA/TM—2015-218924

A First Look at the DGEN380 Engine Acoustic Data From a Core-Noise Perspective

Lennart S. Hultgren
Glenn Research Center, Cleveland, Ohio

National Aeronautics and
Space Administration

Glenn Research Center
Cleveland, Ohio 44135

December 2015

Acknowledgments

This work was supported by the Quiet Performance Subproject of the NASA Fundamental Aeronautics Program Fixed Wing Project. Thanks to Joseph W. Connolly of the NASA GRC Intelligent Control and Autonomy Branch for supplying relevant engine operational parameters obtained from the DGEN Simmot simulation system.

This work was sponsored by the Fundamental Aeronautics Program at the NASA Glenn Research Center.

Level of Review: This material has been technically reviewed by technical management.

Available from

NASA STI Program
Mail Stop 148
NASA Langley Research Center
Hampton, VA 23681-2199

National Technical Information Service
5285 Port Royal Road
Springfield, VA 22161
703-605-6000

This report is available in electronic form at http://www.sti.nasa.gov/ and http://ntrs.nasa.gov/

A First Look at the DGEN380 Engine Acoustic Data From a Core-Noise Perspective

Lennart S. Hultgren
National Aeronautics and Space Administration
Glenn Research Center
Cleveland, Ohio 44135

Abstract

This work is a first look at acoustic data acquired in the NASA Glenn Research Center Aero-Acoustic Propulsion Laboratory using the Price Induction DGEN380 small turbofan engine, with particular emphasis on broadband combustor (core) noise. Combustor noise is detected by using a two-signal source separation technique employing one engine-internal sensor and one semi-far-field microphone. Combustor noise is an important core-noise component and is likely to become a more prominent contributor to overall airport community noise due to turbofan design trends, expected aircraft configuration changes, and advances in fan-noise-mitigation techniques. This work was carried out under the NASA Fundamental Aeronautics Program, Fixed Wing Project, Quiet Performance Subproject.

1 Introduction

Commercial air traffic is expected to significantly increase in the future and, consequently, subsonic transport-aircraft community noise needs to be further reduced in order to minimize the associated negative environmental and economic impacts. For current-generation engines, noise generated in the core by components such as the compressor, combustor, and turbine can be significant contributors to the overall noise signature at low-power conditions, typical of approach flight, but it is typically overwhelmed by jet and fan noise at high engine-power settings during takeoff. However, current design trends and expected technological advances in engine-cycle design as well as noise-reduction methods are likely to increase the relative importance of core noise at all engine-power levels.[1] Consequently, core noise needs to be addressed in order to meet future aircraft noise-reduction goals. In fact, core noise may well set a propulsion-noise floor limiting the effects of future fan and jet noise reduction techniques if not further controlled.

The present work represents a first look at the core-noise aspects of acoustic data acquired in the NASA Glenn Research Center (GRC) Aero-Acoustic Propulsion Laboratory (APPL) using the Price Induction DGEN380 small turbofan engine during July 2014. In particular, this report is concerned with the detection of combustor noise using a source-separation technique. Combustor noise is a low-frequency broadband contributor to the noise generated in the turbofan engine core. It can be a significant aspect of the aft-quadrant overall noise signature at typical approach conditions for today's turbofan engines and it is predicted[1] to make a significant contribution to all certification noise levels for near-future engine designs. Direct measurement of turbofan-engine combustor noise is difficult because of the presence of jet noise in the frequency range of interest. Since flight effects reduce jet noise more than combustor noise,[2] combustor noise can be a significant contributor to aircraft in-flight noise but may be masked by jet noise under the corresponding static-engine test conditions. Summaries of the current status of combustor-noise source modeling, as well as historical perspectives, are given in the review chapters by Mahan and Karchmer[2] and Hultgren et al.[3] as well as in Hultgren.[4]

2 The DGEN380 Testing Program

The DGEN380 testing program was a one day test in the NASA GRC APPL facility. A Price Induction DGEN380 turbofan engine was brought into the anechoic facility mounted on the back on a small flatback truck. The engine controller, engine-internal steady state sensors, and fuel supply were all integrated in the truck-engine assembly. NASA supplied an inflow control device, some acoustic treatment on relevant truck surfaces, two arrays of microphones for

far field and semi-far-field acoustic measurements, as well as a sting-mounted Kulite pressure sensor to meassure the unsteady pressure fluctuations in the core exit nozzle. A system-level in-flight noise prediction, based on the obtained static data, is presented by Berton[5] for a notional twin-engine very light jet (VLJ) aircraft. Berton's[5] report also contains a brief description of the DGEN engine and its target market. The testing program will also be fully described in other forthcoming reports.

3 Experimental Results

The instrumentation layout consisted of 30 microphones arranged on a 12-foor arc and an engine-internal Kulite sensor located in the core exit duct. The microphone distance from the engine is not large enough for the measurements to be truly in the far field, but they are not in the near field either. Consequently, they will be referred to herein as semi-far-field measurements. The signals were bandpass-filtered with the analog filter settings of 50 Hz and 50 kHz. The signals were digitally sampled at 100 kHz for a total observation time of 60 seconds leading to time series with 6 million data points. The pressure time histories at the internal Kulite sensor and the aft-quadrant far-field microphone located in the 130^o polar direction (measured from the inlet) are used herein. Each time series is here analyzed using an FFT length of 8192 points (corresponding approximately to an 12.2 Hz frequency resolution or bin width), Hanning windowing, and a 50 percent data-segment overlap. The resulting narrow-band spectra are then the average of M = 1463 realizations, or instantaneous spectra.

3.1 *Engine-Internal Kulite and Far-Field Microphone Spectra*

Narrowband (12.2 Hz bin width) sound pressure levels, SPL, for the engine-internal kulite and the 130^o semi-far-field microphone are shown in Fig. 1. The results in panels (a) and (h) are without the engine running at the beginning and end of the test and, consequently show the background noise levels for the test. Panels (b) through (g) correspond to the engine-power settings of 47 %, 60 %, 70 %, 80 %, 90 %, and 95.6 %, respectively. For the microphone data, it is clear that the signal to noise ratio, S/N, is very good, except possibly at the very lowest frequencies—but even there, the margin is about 20 dB.

The ambient, or background, noise level for the Kulite measurements is quite high, however. The reason for this is not totally obvious at this point. Some understanding can be obtained by considering the smallest pressure perturbation that can be detected by the pressure transducer and the instrumentation chain. Assuming that proper signal conditioning has been carried out, then this pressure fluctuation is given by

$$(\Delta p)_{min} = P_{FS} \times \max\left(s_I, 2^{-L}\right), \tag{1}$$

where P_{FS} is the full-scale pressure of the transducer, s_I is the transducer relative inaccuracy (the combined effect of nonlinearity, repeatability, and hysteresis), and L is the number of bits used in the analog-to-digital conversion circuitry. The manufacturer's specification sheet lists the combined uncertainty as typically ± 0.1 % of the full scale, i.e. $s_I = 1 \times 10^{-3}$. For 24 bit analog-to-digital conversion (ADC), as used here, $2^{-L} \approx 6 \times 10^{-8}$. Consequently, ADC quantization can be eliminated as the reason for the noise floor. Furthermore, if it is assumed that this error is evenly distributed over all frequencies under consideration, then it follows that the noise floor, or noise pressure level (NPL), is given by

$$\mathrm{NPL} = 10\log\left[\frac{2}{N_{FFT}}\left(\frac{(\Delta p)_{min}}{P_{ref}}\right)^2\right] = 10\log\left[\frac{2}{N_{FFT}}\left(\frac{s_I P_{FS}}{P_{ref}}\right)^2\right] \approx 102.6\,dB, \tag{2}$$

where N_{FFT} is the number of points used in the spectral analysis (twice the number of frequency bins), and $P_{ref} = 2 \times 10^{-5}$ Pa is the reference pressure in SI units. The estimate in Eq. (2) is in line with what can be observed in Fig. 1, thus indicating that transducer quantization is at the source of the high noise level. Furthermore, eventhough the S/N ratio for the Kulite signal is not stellar, it is at least 10 dB for frequencies less than about 1000 Hz, which is the expected range for combustor broadband noise.

3.2 *Combustor-Noise Narrowband Results*

The two-signal coherent-power method[6] is used here to detect the core-noise component of the total noise signature captured by the far-field microphone. Following the notational convention used in Hultgren and Miles,[7] the total measured signals by the engine-internal sensor and the free-stream microphone are denoted by x and y, and the

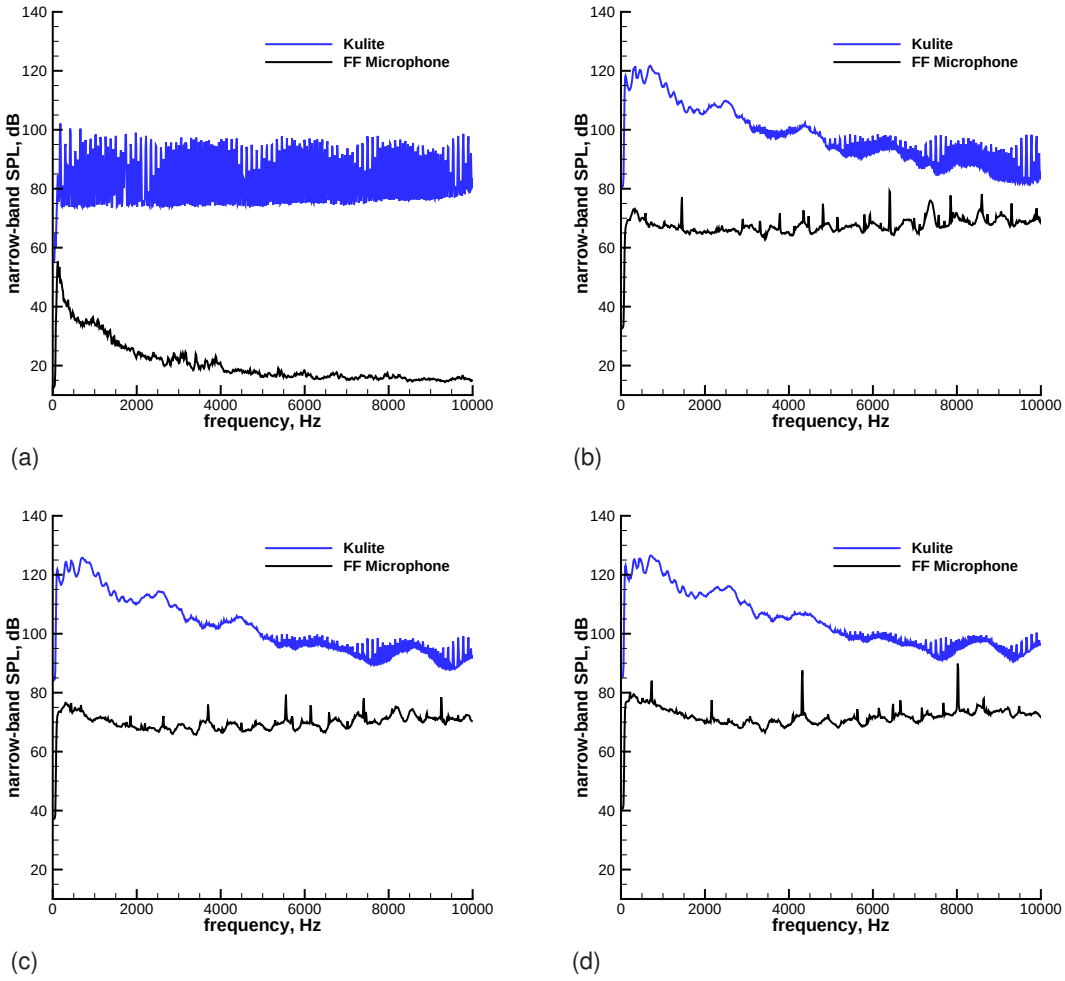

Figure 1. Kulite and 130^o direction far-field microphone narrowband (12.2 Hz) SPL versus frequency; (a): 0 % engine power; (b): 47 % engine power; (c): 60 % engine power; (d): 70 % engine power.

coherent core-noise signals at the same locations are denoted by u and v. It then follows that the coherent output signal is estimated by

$$G_{vv} = \gamma_{xy}^2 G_{yy}\,, \tag{3}$$

where $G_{\alpha\alpha}$, $G_{\alpha\beta}$, $\gamma_{\alpha\beta} = |G_{\alpha\beta}|/\sqrt{G_{\alpha\alpha}G_{\beta\beta}}$ denote the one-sided auto spectrum, cross spectrum, and coherence of the two signals α and β, where α and β are dummy indexes.

Figure 2 shows the 130^o far-field narrowband results obtained using this two-signal source-separation method for various engine power settings. The black, red, and grey curves show the total noise signature G_{yy}, the core-noise component G_{vv}, and the threshold value for the coherent output power $\varepsilon^2 G_{yy}$, where

$$\varepsilon = \sqrt{1-(1-P)^{1/(M-1)}} \tag{4}$$

is a statistical coherence threshold. If the coherence computed from measurements, using M independent averages, is less than ε, then P is the probablity that the two signals are independent, i.e. that the actual coherence is zero. $P = 0.95$ is used herein to establish the threshold value ($\varepsilon \approx 0.0452$).

Figure 2 clearly shows the presence of broadband combustor noise below about 500 Hz. The detected frequency range appears to be shrinking with increasing engine power, but that is only an artifact of the source-separation

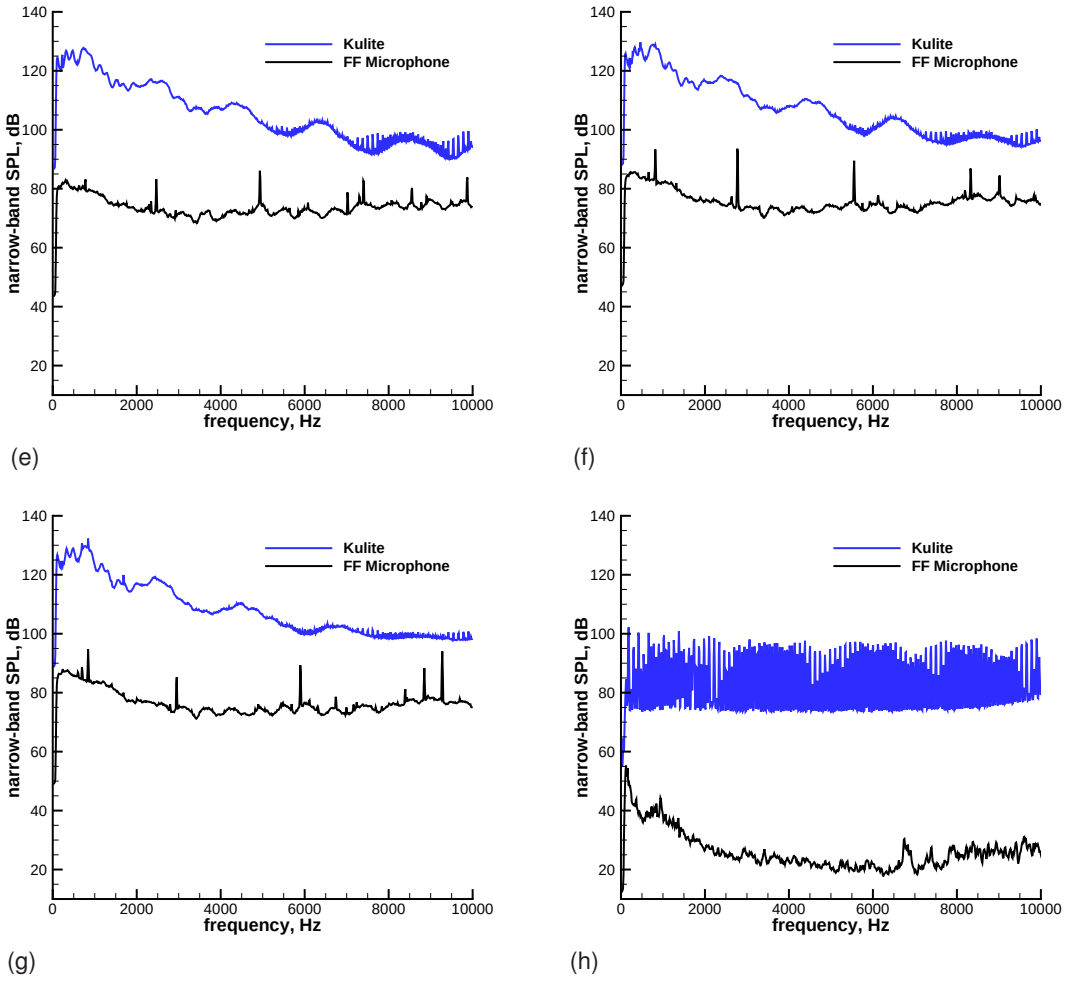

Figure 1, continued. Kulite and 130^o direction far-field microphone narrowband (12.2 Hz) SPL versus frequency; (e): 80 % engine power; (f): 90 % engine power; (g): 95.6 % engine power; (h): 0 % engine power.

method—once the core-noise level falls to about 27 dB below the total signal level ($10\log\varepsilon^2$), it can no longer be detected. In addition, the inherent positive bias error[6,7] in the approximation of the coherent input signal strength used in the two-signal method tends to also lead to an underestimation of the output power, which has been observed to increase in severity with increasing frequency.[7]

Several discreete tones can also be discerened in the spectra. The tones can be more effectively identified, or verified, by employing the deliberate dealignment technique of Miles.[8] This is implemented here by delaying the microphone signal by 16384 data points, which is twice the data segment length. Figure 3 shows the resulting coherence for the six engine power settings under consideration. The red and blue curves represent the computed coherence for aligned signals and deliberately dealigned signals. The gray line indicates the statistical coherence threshold in Eq. (4). The figure shows, as earlier noted by Miles[8], that this threshold is a good estimate even though the data segments stricly speaking are not fully independent when the 50 % overlap technique is employed. The discreete tones are clearly idenfieable in the dealigned cases and are listed in Table 1.

For each power setting, this table lists the shaft speeds for the Low-Pressure Turbine (N_{LPT}) and the High-Pressure Turbine (N_{HPT}) as well as any discrete tones A–E that are observable in the coherence data. The shaft speeds were obtained by averaging engine data (10 Hz sample rate) over the last minute spent at each set point. The instantaneous N_{LPT} tracks the requested set point quite well, with a root-mean-square deviation less than about 7 rpm.

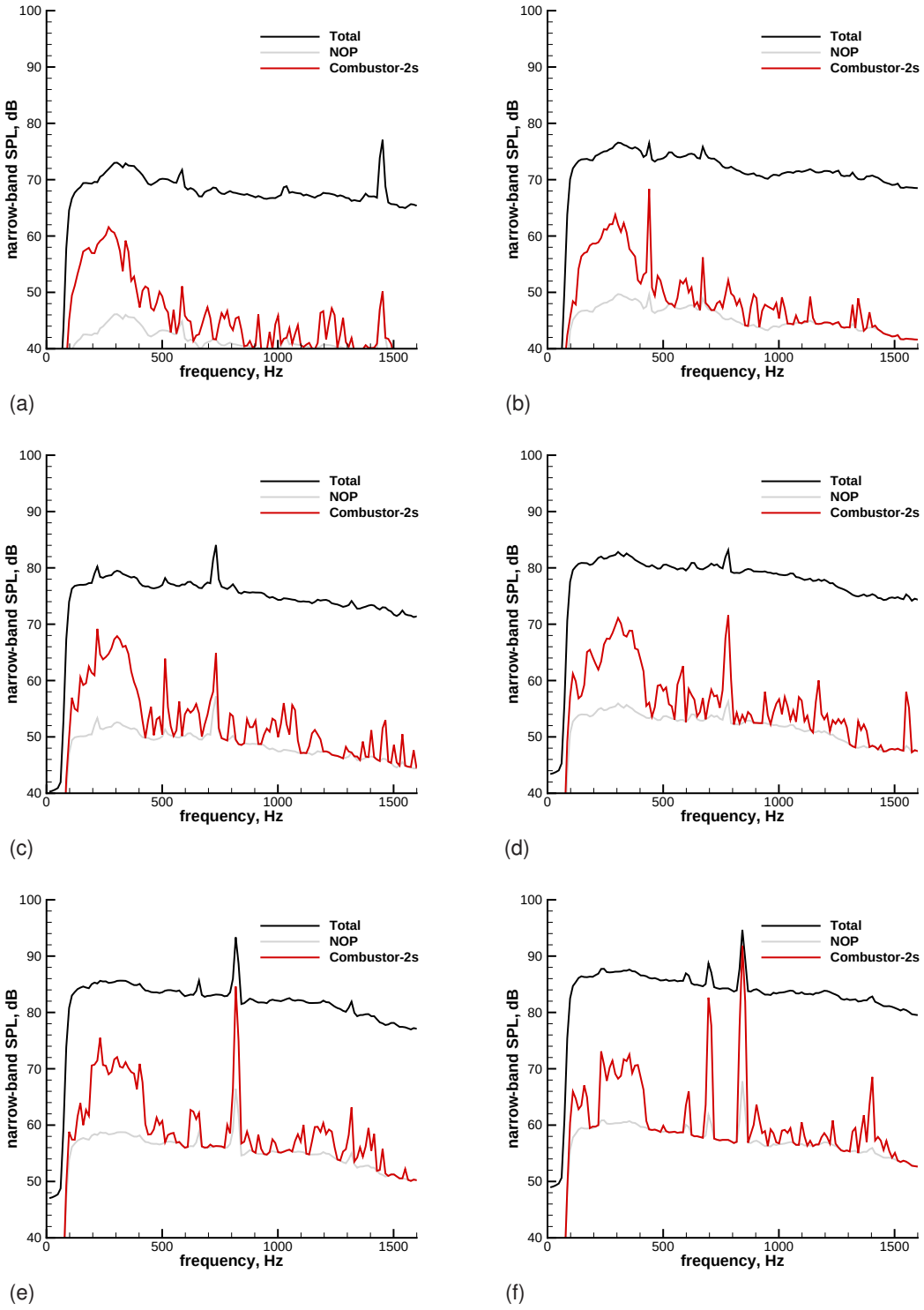

Figure 2. Far-field narrowband (12.2 Hz) SPL in the 130^o direction versus frequency; (a)–(f): black curve—total noise signature; red curve—two-signal-method educed core noise; gray curve—noise floor; engine power: (a) 47 %, (b) 60 %, (c) 70 %, (d) 80 %, (e) 90 %, (f) 95.6 %.

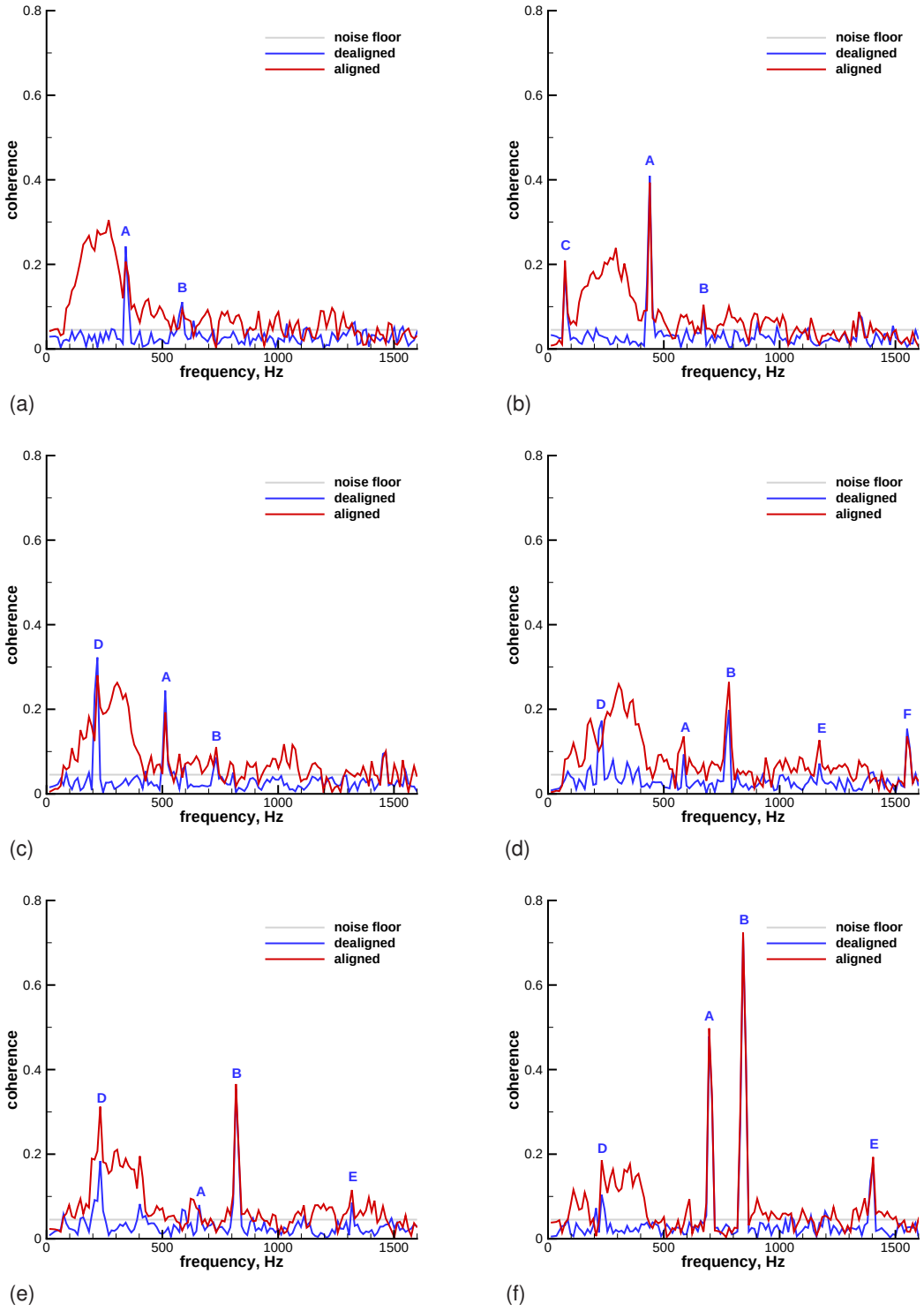

Figure 3. Narrowband (12.2 Hz) coherence between engine-internal sensor and 130^o-direction microphone versus frequency; (a)–(f): red curve—aligned signals; blue curve—deliberately dealigned signals; gray line—noise floor; engine power: (a) 47 %, (b) 60 %, (c) 70 %, (d) 80 %, (e) 90 %, (f) 95.6 %; the tones labeled A–F are listed in Table 1 and explained in the text.

Table 1. Major core-noise tones, Hz

power	N_{LPT}	N_{HPT}	A	B	C	D	E	F
47 %	20506	34806	341.8	585.9				
60 %	26182	40316	439.5	671.4	73.2			
70 %	30545	43691	512.7	732.4		219.7		
80 %	34909	46554	585.9	781.3		231.9	1172	1563
90 %	39271	49076	659.2	817.9		231.9	1318	
95.6 %	41370	50477	695.8	842.3		231.9	1404	

The tones A and B are observable at all the power settings and they are simply the shaft frequencies of the low-pressure and high-pressure turbines, respectively. The tones E and F are the first harmonic of the tones A and B. The tone C is only seen at one condition and could be a combustor rumble tone. The tone D is essentially at a fixed frequency, i.e. independent power setting for the four conditions for which it is seen. It is possible that it is a bleed-valve tone.

Figure 4 shows the phase-angle variation of the cross-spectrum between the engine-internal-sensor signal and the 130^o-far-field-microphone signal over the frequency range relevant to combustor noise. The phase angle is only computed for frequences where the coherence is larger than the threshold given in Eq. (4), i.e. only when $\gamma_{xy} > \varepsilon$. The phase angle is unwrapped (removing the effects of the branch cuts in the arctan function) and then normalized by 2π radians. The red symbols denote the computed normalized, unwrapped phase angle and the black curve is the least-square linear fit to the data,

$$\left[\frac{\arg(G_{xy})}{2\pi}\right]^{(LSF)} = \tau f + b, \tag{5}$$

where τ is the time delay. The good fit in each of the panels indicates, as expected, that there is a constant time delay between the two measuring stations for signals in this frequency range. The so-determined time delays, together with their 95 % confidence intervals, are shown in Table 2. Note that the time resolution from the sampling is 0.01 ms, which is smaller than the one-sided confidence bands. The typical (average) time delay is about 6.9 ms, which for the speed of sound of 345 m/s (1130 ft/s), corresponding to the average ambient conditions during the testing, leads to a virtual travel distance of about 2.4 m (7.8 ft). This virtual distance is, as it should be, smaller than the microphone-array radius since the acoustic waves travel through hotter flow regions where the speed of sound is higher before entering the ambient region.

Table 2. Time delays determined through least-square-fit procedure

power	47 %	60 %	70 %	80 %	90 %	95.6 %
τ, ms	6.91 $\pm$0.05	6.79 $\pm$0.09	6.77 $\pm$0.06	6.89 $\pm$0.06	6.97 $\pm$0.05	6.97 $\pm$0.09

3.3 *Combustor-Noise 1/3-Octave Results*

The narrow-band results of the preceeding subsection are summed up to yield the corresponding 1/3-octave SPL spectra. Figure 5 shows the results for the 1/3-octave frequency range of 100[a] to 1000 Hz for the six power settings. The black, red, and grey symbols denote the total signature, the combustor-noise component, and the threshold value for the source-separation method. Any combustor-noise results below the latter would not be meaningful using the present source separation and data processing techniques. The presence of broadband combustor noise up to about 500 Hz is evident in all of the panels, (a)–(f). The distinct shaft-frequency tones, A and B, clearly affect the 1/3-octave spectra above about 500 Hz for the three highest power settings, (d)–(f).

[a]Lower frequency bands are affected by roll-off effects of the high-pass filter at 50 Hz and, consequently, are not shown in the figure.

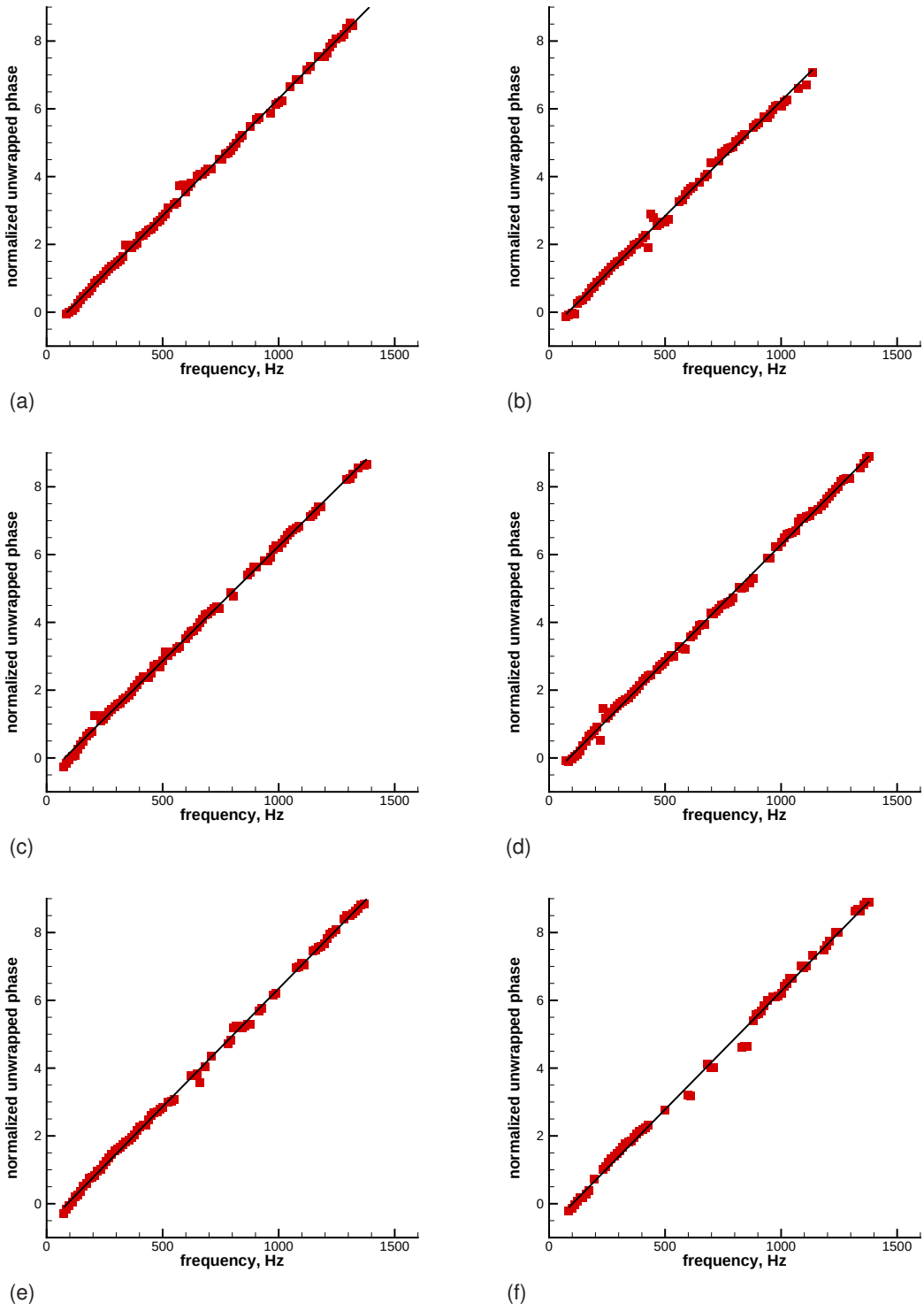

Figure 4. Unwrapped and normalized, engine-internal sensor and 130^o-direction microphone cross-spectrum phase versus frequency; (a)–(f): red symbols—cross-spectrum phase; black line—least-square linear fit; engine power: (a) 47 %, (b) 60 %, (c) 70 %, (d) 80 %, (e) 90 %, (f) 95.6 %.

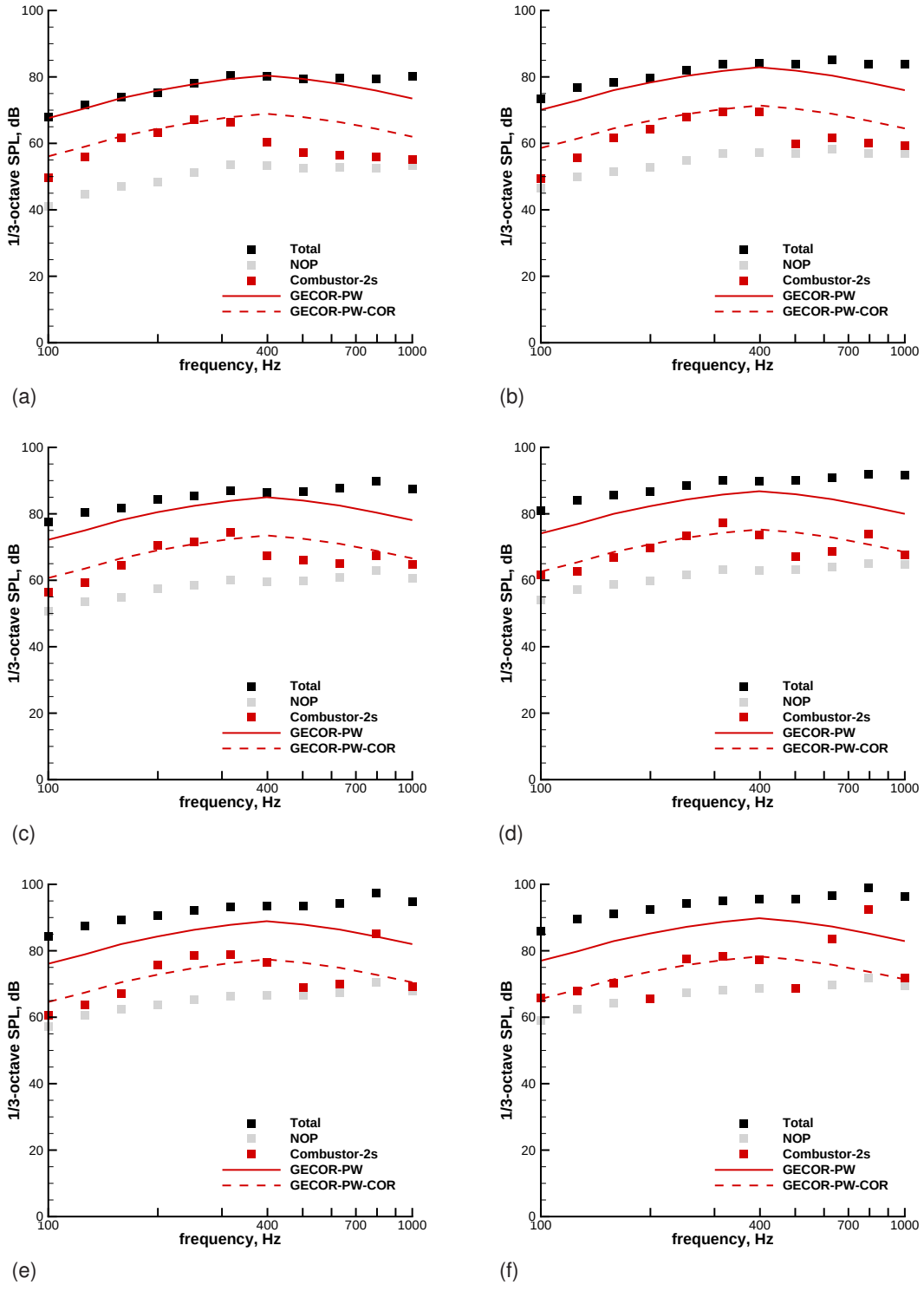

Figure 5. Total and combustor-noise far-field 1/3-octave SPL in the 130^o-direction versus 1/3-octave-band center frequency; (a)–(f): black symbols—total noise signature; red symbols—combustor-noise component; and gray symbols—noise floor; engine power: (a) 47 %, (b) 60 %, (c) 70 %, (d) 80 %, (e) 90 %, (f) 95.6 %.

The solid lines in Fig. 5 represent ANOPP 1/3-octave SPL predictions for the combustor noise using the small-engine (SmE) method with the PW turbine attenuation formula, SmE-PW. See the Appendix for more information about the combustor-noise models in ANOPP. Clearly these curves overpredict the educed combustor noise. The dashed curves represent the ANOPP 1/3-octave SPL predictions for the combustor noise after applying a thrust-class correction. The proposed thrust-class correction is based on the thrust ratio of the two engine classes, very small engines (VSE) and small engines (SmE), and leads to a change in the total acoustic power level of -11.5 dB. By applying this thrust-class correction to the ANOPP SmE-PW predictions, the results (dashed curves) compares well with data for all the conditions of the full-engine test. Using a thrust-class correction is not without precedent since this is really the difference between the original SAE method (1970s) and the newer small-engine method (1990s) in the GECOR module of ANOPP.

4 Summary and Conclusions

A first analysis of the broadband combustor (core) noise component of the acoustic data acquired in the NASA GRC APPL facility using the Price Induction DGEN380 small turbofan engine has been performed. Combustor noise was detected by using a two-signal source separation technique employing one engine-internal sensor and one semi-far-field microphone. Broadband combustor noise is clearly present in the microphone data below about 500 Hz and is likely to be present also up to about 1000 Hz even though it was not detected by the source separation technique in this higher frequency range due to the inherent limitations of the technique. Several low-frequency discrete tones were also discerned in the core-noise signature. ANOPP GECOR predictions (i.e. combustor noise only) for the static-engine test were carried out using relevant engine-operational parameters. By applying a thrust-class correction to the predictions they compare well with data for all the conditions of the full-engine test. Using a thrust-class correction is not without precedent since this is really the difference between the original SAE method (1970s) and the newer small-engine method (1990s) in the GECOR module of ANOPP. The interim scaling is based on the thrust ratio of the different engine classes and appears to give satisfactory results. This preliminary finding is subject to further evaluation and might change if and when more engine data becomes available.

Appendix ANOPP GECOR 1/3-Octave Combustor-Noise Models

Combustor-noise prediction in the semi-empirical NASA Aircraft Noise Prediction Program (ANOPP)[9,10] is provided by the GECOR subroutine. The current module (ANOPP L30v3) essentially contains two basic models with variations. The first model is fully 1/3-octave based and in its original implementation[11,12] is customarily referred to as the SAE method. This method also contains a small-engine revision[13] (referred to as SmE herein) as well as an option for an alternate turbine-transmission-loss formula.[2,4,14–16] The second class of models, that will not be further discussed or utilized here, has an intermediate-narrow-band formulation[17] in order to account for tail-pipe resonances.

For a static-engine test, the (dimensional) combustor-noise mean-square pressure in each 1/3-octave band (b) is given by

$$< p^2 >^{(b)} = \frac{\rho_\infty c_\infty \Pi D(\theta) S(f_b)}{4\pi r_s^2} \tag{A 1a}$$

for both the SAE and SmE methods in ANOPP, where r_s is the distance between the source and the observer and ρ_∞ and c_∞ are the ambient density and speed of sound. $D(\theta)$ is a directivity function that depends only on the polar angle θ and satisfies the normalization condition

$$\int_0^\pi D(\theta) \sin\theta \mathrm{d}\theta = 2\,. \tag{A 1b}$$

$S(f_b)$ is a spectrum function satisfying

$$\sum_b S(f_b) = 1 \tag{A 1c}$$

and f_b is the 1/3-octave-band center frequency. Π is the total acoustic power

$$\Pi = \int_A \frac{\sum_b < p^2 >^{(b)}}{\rho_\infty c_\infty} \mathrm{d}A\,, \tag{A 1d}$$

where $\mathrm{d}A = r_s^2 \sin\theta \mathrm{d}\theta \mathrm{d}\phi$, with ϕ denoting the azimuthal angle. The sound pressure level $SPL^{(b)}$ in an 1/3-octave frequency band, the overall sound pressure level *OASPL*, and the power level *PWL* are given by

$$SPL^{(b)} = 10\log(< p^2 >^{(b)} / p_{ref}^2)\,, \tag{A 2a}$$

$$OASPL = 10\log(\sum_b < p^2 >^{(b)} / p_{ref}^2) = 10\log[\rho_\infty c_\infty \Pi D(\theta)/4\pi r_s^2 p_{ref}^2]\,, \tag{A 2b}$$

$$PWL = 10\log(\Pi/\Pi_{ref})\,, \tag{A 2c}$$

where $p_{ref} = 2\times10^{-5}$ Pa and $\Pi_{ref} = 1\times10^{-12}$ W if SI units are used. The ANOPP GECOR formula for the total acoustic power is

$$\Pi = 10^{K/10} c_\infty^2 \dot{m}_{core} \left(\frac{T_{t,ce} - T_{t,ci}}{T_{t,ci}}\right)^2 \left(\frac{P_{t,ci}}{P_\infty}\right)^2 \times F_{TA}\,, \tag{A 3a}$$

where the constant $K = -60.53\ldots$ in the SAE method and $K = -64.53\ldots$ in the SmE method. $\dot{m}_{core}$ is the mass flow rate into the combustor, $T_{t,ci}$ and $T_{t,ce}$ are the total temperature at the combustor inlet and exit, $P_{t,ci}$ is the total combustor-inlet pressure, and P_∞ is the reference (static) pressure. The reference state is ambient conditions, actual or standard sea-level values. *Note that the only difference between the SAE and SmE methods is the value of the constant K leading to a 4 dB difference in the acoustic power level!*

F_{TA} is a turbine attenuation, or loss, factor and, in the original formulation, is given by [18]

$$F_{TA} = \left(\frac{\Delta T_{des}}{T_\infty}\right)^{-4}\,, \tag{A 3b}$$

where ΔT_{des} is the design-point temperature drop across the turbine[b] and T_∞ is the reference temperature. Note that the acoustic transmission loss is independent of the engine operating condition with this formulation. The GECOR module recently has been updated to also have an option to use an alternative turbine-transmission-loss formula, namely the simplified[2] Pratt & Whitney [14,15] acoustic-turbine-loss formula,

$$F_{TA} = \frac{0.8\zeta}{(1+\zeta)^2}\,, \tag{A 3c}$$

where ζ is the ratio of the characteristic impedances across the turbine, i.e. $\zeta = \rho_{te}c_{te}/\rho_{ti}c_{ti}$ with ρ and c denoting density and speed of sound, respectively, and the subscripts 'te' and 'ti' indicating turbine exit and inlet. With this formulation, the turbine acoustic transmission loss depends on the engine operation conditions since the impedance ratio does. Hultgren [16,c] found that predictions using this formula compared well with data for flight idle, approach, cutback, and takeoff power settings from a full-scale static-engine test. [19] Eqs. (A 3b) and (A 3c) will be referred to as the GE and PW turbine-transmission-loss formulas, respectively. Note that both these loss formulas are frequency independent.

REFERENCES

[1] J. B. Berton, E. Envia, and C. L. Burley. An analytical assessment of NASA's N+1 Subsonic Fixed Wing project noise goal. Technical Report AIAA Paper 2009-3144, 16th AIAA/CEAS Aerocoustics Conference, Miami, Florida, 2009.

[b] If this value is not available, the corresponding takeoff value can be used.

[c] Due to a typographical error, Eq. 13 in Hultgren [16] corresponding to Eq. (A 3c) here is inverted, but the computations therein are correct.

[2] R. J. Mahan and A. Karchmer. Combustion and core noise. In H. H. Hubbard, editor, *Aeroacoustics of Flight Vehicles: Theory and Practice*, volume 1, chapter 9, pages 483–517. NASA Reference Publication 1258, WRDC Technical Report 90-3052, 1991.

[3] L. S. Hultgren, J. H. Miles, and P. C. E. Jorgenson. Engine system and core noise. In M. D. Dahl, editor, *Assessment of NASA's Aircraft Noise Prediction Capability*, chapter 3, pages 35–62. NASA TP-2012-215653, 2012.

[4] L. S. Hultgren. A comparison of combustor-noise models. Technical Report AIAA Paper 2012-2087 (NASA/TM-2012-217671), 18th AIAA/CEAS Aerocoustics Conference, Colorado Springs, Colorado, 2012.

[5] J. J. Berton. System noise prediction of the DGEN 380 turbofan engine. Technical Report AIAA Paper 2015-2516, 21st AIAA/CEAS Aeroacoustic Conference, Dallas, Texas, 2015.

[6] J. S. Bendat and A. G. Piersol. *Engineering Applications of Correlation and Spectral Analysis*. Wiley-Interscience, 1980.

[7] L. S. Hultgren and J. H. Miles. Noise-source separation using internal and far-field sensors for a full-scale turbofan engine. Technical Report AIAA Paper 2009-3220 (NASA TM-2009-215834), 15th AIAA/CEAS Aeroacoustic Conference, Miami, Florida, 2009.

[8] J. H. Miles. Aligned and unaligned coherence: A new diagnostic tool. Technical Report AIAA Paper 2006-0010 (NASA TM-2006-214112), 44th Aerospace Sciences Meeting, Reno, Nevada, 2006.

[9] W. E. Zorumski. Aircraft noise prediction program theoretical manual, part 1. Technical Report NASA TM-83199-Pt-1, NASA, 1982.

[10] W. E. Zorumski. Aircraft noise prediction program theoretical manual, part 2. Technical Report NASA TM-83199-Pt-2, NASA, 1982.

[11] J. J. Emmerling, S. B. Kazin, and R. K. Matta. Core engine noise control program, Volume III, Supplement 1—Prediction methods. Technical Report FAA RD-74-125 III-I, FAA, 1976.

[12] P. Y. Ho and V. L. Doyle. Combustion noise prediction update. Technical Report AIAA Paper 1979-0588, 5th AIAA Aerocoustics Conference, Seattle, Washington, 1979.

[13] J. W Hough and D. S. Weir. Small engine technology (SET)—Task 13 ANOPP noise prediction for small engines: Jet, core, and turbine module revisions. Technical Report No. 21-9655, AlliedSignal Engines, Phoenix, Arizona, 1997.

[14] D. C. Mathews, N. F. Rekos, Jr, and R. T. Nagel. Combustion noise investigation. Technical Report FAA RD-77-3, FAA, 1977.

[15] D. C. Mathews and N. F. Rekos, Jr. Prediction and measurement of direct combustion noise in turbopropulsion systems. *J. Aircraft*, 14(9):850–859, 1977.

[16] L. S. Hultgren. Full-scale turbofan-engine turbine-transfer function determination using three internal sensors. Technical Report AIAA Paper 2011-2912 (NASA TM-2012-217252), 17th AIAA/CEAS Aeroacoustic Conference, Portland, Oregon, 2011.

[17] B. Schuster and L. Lieber. Narrowband model for gas turbine engine combustion noise prediction. Technical Report AIAA Paper 2006-2677, 12th AIAA/CEAS Aerocoustics Conference, Cambridge, Massachusetts, 2006.

[18] R. Motsinger. Prediction of engine combustor noise and correlation with T64 engine low frequency noise. Technical Report R72AEG313, General Electric Co., 1972.

[19] D. S. Weir. Engine validation of noise and emission reduction technology phase I. Technical Report NASA CR-2008-215225, NASA, 2008. Honeywell Report No. 21-13843, Honeywell Aerospace, Phoenix, Arizona.